Communication

Characteristics of TCDA With Polarization Converting Ground Plane

Seongjung Kim and Sangwook Nam

***Abstract*—In this study, we propose a tightly coupled dipole array (TCDA) with a polarization convertor (PC) to overcome the bandwidth limitation at $h = 0.5\ \lambda$ and $1\ \lambda$ of a conventional TCDA. Ultrawideband and low-profile array antennas are gaining considerable attention with widespread of wireless electronic systems. Although TCDA has such characteristics and several advantages compared with others, their bandwidth is still limited by the ground plane (GP) reflection. The use of resistive frequency selective surface (FSS) to overcome this limitation entails ohmic losses which deteriorate the radiation efficiency of the array antenna. In the present study, we propose a 20.9:1 TCDA antenna without resistive FSS. The proposed array antenna employs a PC to overcome the limitation of bandwidth due to GP reflection when the height of the array antenna is $0.5\ \lambda$ and $1\ \lambda$. The concept neither involves any dielectric superstrates nor does it introduce any resistive loss. Thus, beam steering is possible without surface wave generation. As a result, the proposed array antenna is expected to be successfully applied to wideband and beam-scannable array with improved performance of wireless electronic devices.**

***Index Terms*—Low-cost, low-profile, low-weight, phased array, polarization conversion, tightly coupled dipole array (TCDA), wideband.**

I. Introduction

Ultrawideband and electrical beam-scannable phased array antennas with low profile are in high demand for many wireless electronic systems. One of these antennas is a Vivaldi antenna [1]. However, it has a high-profile structure. The patch antennas are low profile [2], but their bandwidth is narrow. Uniform amplitude current sheet array (CSA) in free space ideally has infinite impedance bandwidth (IBW) [3] and tightly coupled dipole array (TCDA) imitating CSA has been designed in recent years due to its many attractive features such as low profile and ultrawideband, even on the ground plane (GP) [4]–[9]. Nevertheless, the bandwidth of TCDA is still limited by the GP reflection whenever the height of the array antenna becomes an integer multiple of a half wavelength. Some studies have overcome this by introducing the resistive frequency selective surface (FSS) [10], [11]. Although this can increase the bandwidth, additional ohmic losses more than 3 dB also occur. To reduce these ohmic losses, a complimentary superstrate is introduced. This has been known to reduce ohmic losses to −1.4 to −1.1 dB, where the relative dielectric constant of complimentary superstrate is 4 [12]. However, the high dielectric superstrate can incur the surface waves that, in turn, limit the scan-angle [13]. In addition, a dielectric superstrate inevitably increases the height of array antenna, making it bulky, heavy, and expensive.

Manuscript received November 20, 2019; revised July 25, 2020; accepted August 17, 2020. Date of publication August 31, 2020; date of current version April 7, 2021. This work was supported in part by the Bio-Mimetic Robot Research Center Funded by Defense Acquisition Program Administration and in part by Agency for Defense Development under Grant UD190018ID. *(Corresponding author: Seongjung Kim.)*

The authors are with the School of Electrical and Computer Engineering, Institute of New Media Communication (INMC), Seoul National University, Seoul 08826, South Korea (e-mail: sjkim@ael.snu.ac.kr; snam@snu.ac.kr).

Color versions of one or more of the figures in this communication are available online at https://ieeexplore.ieee.org.

Digital Object Identifier 10.1109/TAP.2020.3019399

In this communication, the characteristics of TCDA replacing the GP to a polarization convertor (PC) is investigated. It is a special approach to avoid the GP reflection without inducing any ohmic losses. The potential problems in [12], particularly ohmic losses and surface wave, can be addressed. Our study can help improve radiation efficiency from −1.4 to −1.1 dB to −0.7 to 0.0 dB. Furthermore, in contrast with the structure presented in [12], the proposed structure helps reduce the weight and cost of the antenna since it does not employ the superstrate. Furthermore, the proposed array operates successfully at low frequency bands by employing the perfect electric conductor (PEC) side walls even though it has a small finite size of 4 × 4 TCDA. In fact, the introduction of the PC generates high cross-polarization which is not favorable in general. However, the polarization purity of an antenna may not be critical for easily depolarizing applications, such as mobile communications. Thus, it can be utilized for polarization-insensitive systems as an ultrawideband array antenna. In addition, if the proposed array antenna is rotated by 90°, the orthogonal polarization can be obtained and used to increase the diversity gain of communication systems.

The communication is organized as follows: In Section II, the characteristics of the proposed unit cell antenna is described by an equivalent circuit. In Section III, the performance of a 4 × 4 finite array antenna composed of the proposed unit is presented; performances include array gain, beam patterns, and beam scanning. In Section IV, conclusions are drawn from the study.

II. Development and Description of the Proposed Unit Cell Antenna

In this section, we present the development of the proposed unit cell antenna and explain two advantages obtained by introducing the PC. In the beginning, the impedance characteristics of TCDA in free space and TCDA with a GP are described. Next, we explain the PC design to convert polarization, which can neutralize the effect of GP reflection, so that the antenna acts like in free space. Finally, we combine the PC and the TCDA. Then, we show how the limitation of the high-frequency band is overcome. In the last discussion of this section, by introducing the PC, it is shown that a superstrate is not needed for impedance matching. All electromagnetic (EM) simulations were performed via Computer Simulation Technology (CST-2018).

Fig. 1(a) shows the unit cell of TCDA. Fig. 1(b) and (c) shows the equivalent circuits of Fig. 1(a) with and without the GP, respectively. All PCB boards are FR-4 ($\varepsilon_r = 4.3$, $tan\delta = 0.025$) and the thickness is 1.6 mm. The 120 Ω discrete port is used at the center of the dipole. $Y_{air} = \sqrt{\varepsilon_0/\mu_0} = 1/377$ is the characteristic admittance of the virtual waveguide [3]. The coupling capacitance C_1 of the equivalent circuit can be obtained by extracting the odd mode capacitance by putting a PEC wall at the center of gap between two dipole arms. The self-inductance of dipole, L_1 can be found by (1) [14]. The self-capacitance, C_2, and the inductance of the dipole, L_2, introduced by Riviere and coworkers [16] are calculated by two different

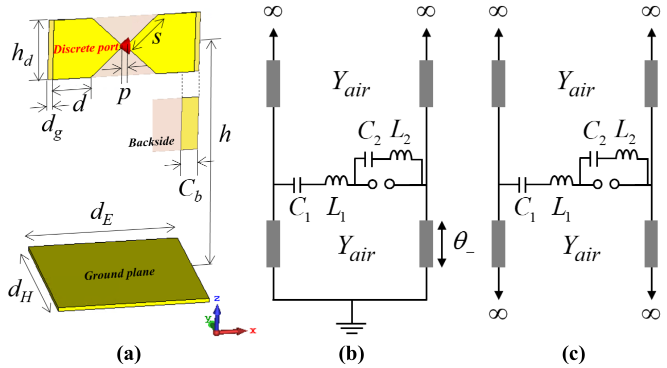

Fig. 1. (a) Unit cell of TCDA which is periodic with d_E along x-axis and d_H along y-axis, (b) equivalent circuit with GP of height h, and (c) without GP ($p = 1$ mm, $s = 35.36$ mm, $C_b = 15$ mm, $h_d = 50$ mm, $d = 30.75$ mm, $d_g = 4$ mm, $d_E = 120$ mm, $d_H = 120$ mm, $h = 185$ mm).

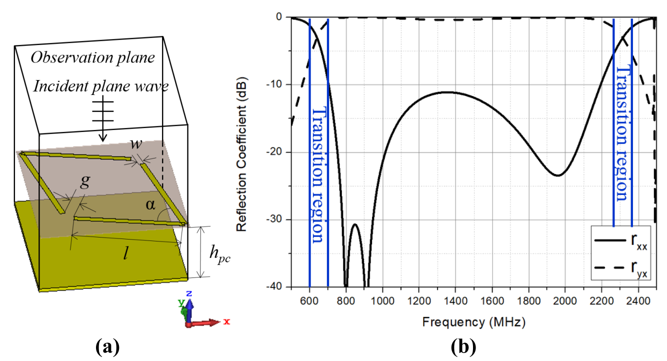

Fig. 2. PC unit cell at the height h_{pc} is on the xy-plane with the proper periodic conditions. (a) Unit cell of PC. (b) Reflection coefficient at the broadside direction. r_{xx} is the reflection of x to x polarization and r_{yx} is the reflection of x to y polarization. ($h_{pc} = 50$ mm, $g = 8.28$ mm, $w = 4.5$ mm, $l = 88$ mm, $\alpha = 65°$).

self-resonance frequencies by the following equations:

$$L_1 = \frac{\mu_0 l_d}{4\pi} \ln \frac{2l_d}{a_e} \tag{1}$$

$$C_2 = \frac{1}{L_1}\left(\frac{d_E}{\pi c}\right)^2 \tag{2}$$

$$L_2 = \frac{1}{C_2}\left(\frac{d_E}{2\pi c}\right)^2 \tag{3}$$

where c is the speed of light in vacuum, a_e is the equivalent radius of a flat dipole [15], $l_d = 2d$, and μ_0 is the permeability of vacuum. Initial values of these four parameters are calculated and optimized to be fit with full wave simulation of TCDA in free space. $L_1 = 14.75$ nH, $C_1 = 9.12$ pF, $L_2 = 20.02$ nH, and $C_2 = 0.242$ pF. In general, the bandwidth of TCDA in free space is limited by C_1 at low-frequency band and limited by the resonance of C_2 and L_2 at high-frequency band which is at 2287 MHz in this design. As a result, very large bandwidth can be obtained if we choose large C_1 and small C_2.

Fig. 1(b) shows the unit cell and the equivalent circuit of TCDA on the GP where h and θ_- are the physical and electrical lengths, respectively, between TCDA dipole antenna and GP.

Fig. 2(a) shows the unit cell of PC that is periodic on the xy-plane. The operating bandwidth of the proposed PC is improved to 3.14:1 by modifying the design at a bandwidth of 2.25:1 [17]. When the x-polarized plane wave is incident on the PC along the broadside direction, the polarization is converted to y-direction at 700–2200 MHz, as shown in Fig. 2(b).

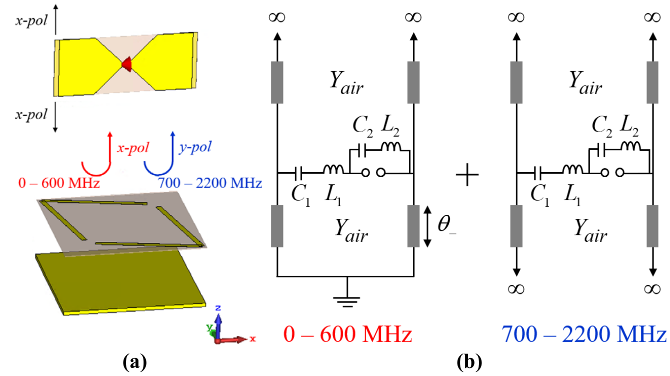

Fig. 3. Proposed unit cell. (a) Structure of the proposed unit cell antenna. (b) Equivalent circuit of the proposed antenna at different frequency bands.

Fig. 3 shows the proposed unit cell and its equivalent circuit of TCDA which is the combination of TCDA and PC shown in Figs. 1(a) and 2(a), respectively. From 0 to 600 MHz, the equivalent circuit is same as that given in Fig. 1(b) since the PC acts as GP. From 700 to 2200 MHz, the equivalent circuit is shown in Fig. 1(c). The reflected wave from the PC, whose polarization is rotated, cannot be coupled to the dipole due to the orthogonal polarization. As a result, the TCDA overcomes not only the high-frequency band limitation at 811 MHz but also at 1622 MHz, which are $h = 0.5\ \lambda$ and $h = 1\ \lambda$, respectively. This can be confirmed by the impedance matching characteristic shown in Fig. 4: without the PC, the IBW for voltage standing wave ratio (VSWR) < 3 is 92–688 MHz (7.48:1), whereas it is 98–1854 MHz (18.9:1) by introducing the PC to the TCDA. Herein, dipole and PC are used to obtain extremely wideband array antenna.

In Fig. 4, the EM simulation results of the proposed unit cell (solid line) are shown to agree well with those of the proposed equivalent circuits except in the transition region (600–700 MHz). This is because both x- and y-polarized waves are reflected from the PC in this region; this cannot be accurately represented by the proposed equivalent circuits. Fig. 5(a) shows the proposed unit cell consisting of a dipole and 100 Ω coplanar strip feed line. Fig. 5(b) shows its matching characteristics for the reference impedance of 100 Ω. To match the 50 Ω SMA connector, the impedance should be halved using the ultrawideband balun (MABA-010247-2R1250). The IBW for VSWR < 3 is 98–1854 MHz (18.9:1) which corresponds to the height of antenna $h + h_d/2 = 0.072\ \lambda_{\text{low}}$ at the lowest operating frequency.

Fig. 6 shows the unit cell of TCDA with a superstrate which is the Taconic TLY-5 ($\varepsilon_r = 2.2$, $tan\delta = 0.0009$). θ_+ is the electrical length of the superstrate of height h_{sup}. $Y^+ = Y_{air} + Y_{sup}$, $Y^- = -jY_{air}cot\theta_-$ and $Z_{in} \approx j\omega L_1 + 1/(j\omega C_1) + 1/(Y^+ + Y^-)$ at low and middle frequency band. For TCDA without a superstrate, $Real\{1/(Y^+ + Y^-)\}$ is equal to $1/Y_{air}$ (=377 Ω) when the θ_- is quarter wavelength and it is hard to match the impedance to 50 Ω. Therefore, many people have employed a superstrate to TCDA since it can reduce the $Real\{1/(Y^+ + Y^-)\}$ when θ_- is quarter wavelength [4], [6], [8]. However, the roles of superstrate mentioned above are not required to the proposed antenna because the reactive energy reflected from the GP does not interact with dipole and the $Real\{1/(Y^+ + Y^-)\}$ is half of 377 Ω in all the operating band of PC. Therefore, the proposed antenna does not need a superstrate for impedance matching which results in a low-weight and low-cost antenna.

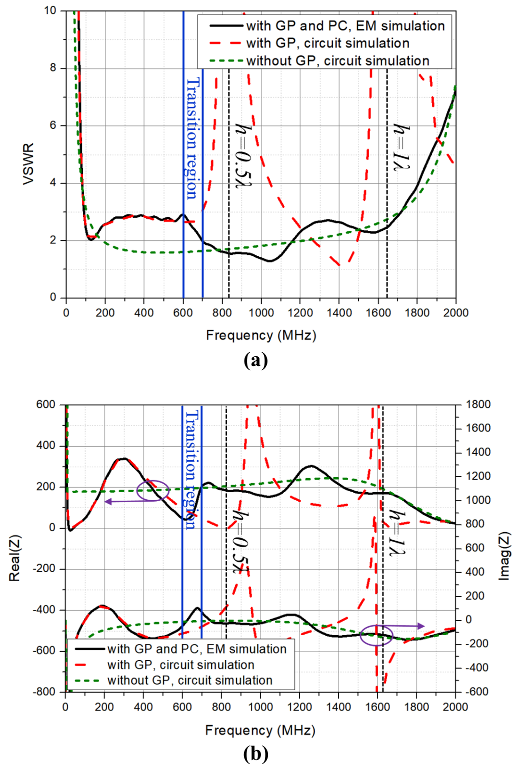

Fig. 4. Comparison with circuit simulations with and without the GP. The black solid line follows the red dotted line from 0 to 600 MHz and the green dotted line from 700 to 2000 MHz. (a) VSWR and (b) antenna input impedance.

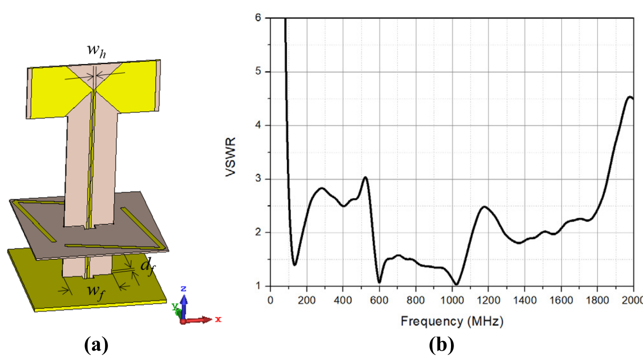

Fig. 5. Proposed antenna combined with the feeding line. (a) Structure of the proposed antenna with feeding line. (b) VSWR of proposed antenna. ($w_h = 1.5$ mm, $w_f = 45$ mm, $d_f = 3.3$ mm).

III. Simulated and Experimental Results for the 4 × 4 Finite Array Antenna

In this section, the 4 × 4 finite array antenna composed of the proposed unit cells is presented and the performances of gain, beam patterns, and beam scanning are studied. For the finite array simulation, the discrete ports (differential ports) are used for simplicity and the insertion loss of balun chip is included to the realized gain. In order to reduce the boundary effects of finite array, we introduced the PEC side walls at the end of E-plane of the array as shown in Fig. 7 which is similar to the case of unit element [18]. In addition, the GPs are extended by w_{ext} along the E-plane.

Fig. 8 shows the pictures of prototype 4 × 4 array antenna. The baluns can be seen under the GP.

Fig. 9 shows the active VSWR for the center element of the 4 × 4 finite array. Measured VSWR is derived by active reflection

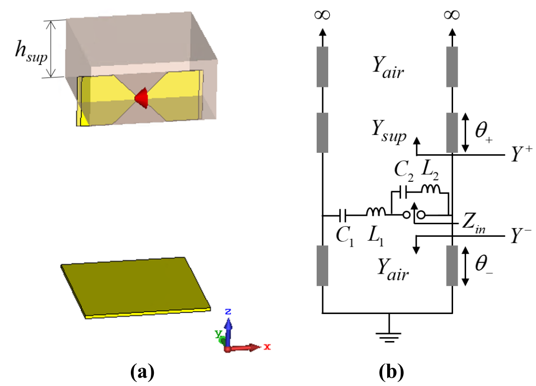

Fig. 6. (a) Unit cell of TCDA and the superstrate with a thickness of h_{sup}. (b) Equivalent circuit of the unit cell with the superstrate.

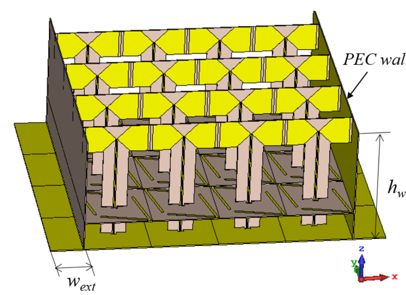

Fig. 7. Proposed 4 × 4 finite array antenna. The GP is extended by w_{ext} on each side. The PEC walls with the height of h_{wall} are introduced on each side to reduce the boundary effects of the finite array. ($w_{ext} = 60$ mm, $h_{wall} = 220$ mm).

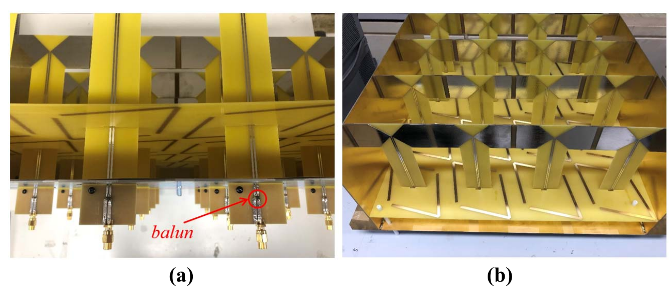

Fig. 8. Photos of fabricated antenna. (a) Front and (b) top view.

coefficient as given by the following equation [19]:

$$\Gamma_i(\theta_0,\ \phi_0) = \sum_{n=1}^{N} S_{i,n}\, a_n \exp\{-jk_0(xd_E \sin\theta_0 \cos\phi_0 + yd_H \sin\theta_0 \sin\phi_0)\} \quad (4)$$

where $S_{i,n}$ is the measured complex coupling coefficients between element i and the nth element of the array, a_n is the complex excitation coefficient of the radiating nth element, N is the total number of elements, k_0 is the free-space wavenumber. For the broadside radiation, the simulated VSWR shows IBW of 90–1778 MHz (19.8:1) and measured VSWR shows IBW of 91–1901 MHz (20.9:1). In fact, it is found that the scan range is limited by the characteristics of the PC which works for narrow incidence angles.

Fig. 10 shows the simulated and measured power gain pattern (black) $G_{array}(\theta, \phi)$, copolarization gain pattern (red) $G^{co}_{array}(\theta, \phi)$, and cross-polarization gain pattern (blue) $G^{cr}_{\mathrm{array}}(\theta, \phi)$ from scanning the beam up to 30° on the E-, D-, and H-planes. The copolarization

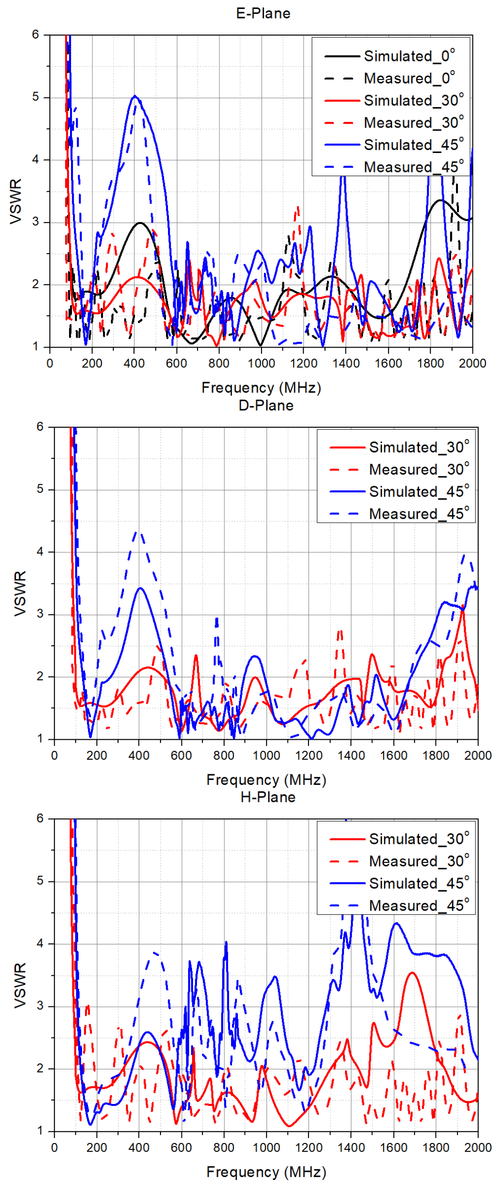

Fig. 9. Simulated and measured active VSWRs of the proposed 4 × 4 finite array antenna on the E-plane ($\phi = 0°$), D-plane ($\phi = 45°$), and H-plane ($\phi = 90°$).

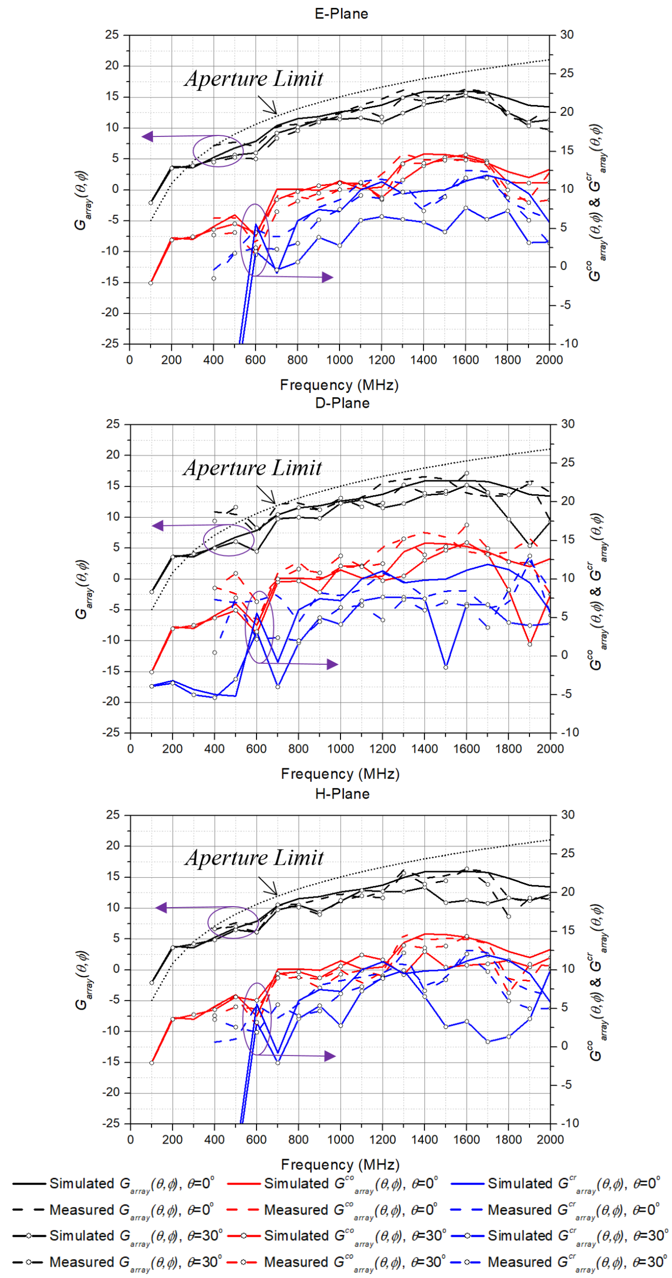

Fig. 10. Simulated and measured array gain of the proposed 4 × 4 finite array antenna with scanning the beam up to 30° on the E-plane ($\phi = 0°$), D-plane ($\phi = 45°$), and H-plane ($\phi = 90°$). The aperture limit is calculated by $4\pi \mathrm{NA}/\lambda^2$ where N is a number of the elements: 16 and A is physical aperture size of unit element: 120 × 120 mm^2.

and cross-polarization patterns are obtained using Ludwig's third definition as follows [20]:

$$e^{co}(\theta,\phi) = \vec{e}(\theta,\phi)\cdot(\hat{\theta}\cos\phi - \hat{\phi}\sin\phi) \tag{5}$$
$$e^{cr}(\theta,\phi) = \vec{e}(\theta,\phi)\cdot(\hat{\theta}\sin\phi + \hat{\phi}\cos\phi) \tag{6}$$

where $\vec{e}(\theta,\phi)$ represents the far electric field of the array antenna. The definition of array gain follows realized gain, which considers impedance mismatch and any ohmic losses including that from the balun chip. The gain was measured by superposition of the active element pattern [21] using the following equation:

$$E(\theta,\phi) = \sum_{i=1}^{N} V_i g_i(\theta,\phi) \tag{7}$$

where V_i is the complex value of excitation, i is the port number, and $g_i(\theta,\ \phi)$ is the complex active element gain pattern of the ith element. The beam can be steered by controlling the phase of V_i.

Until 500 MHz, the cross-polarization gain is considerably less than copolarization gain. However, from 600 MHz onward, the gain of cross-polarization is comparable with copolarization while the gain of copolarization is decreased because of the polarization conversion. In addition, $G_{array}(\theta,\ \phi)$ increases progressively with frequency and the maximum gain is 15.9 dBi within the operating band when scanning the broadside direction. When scanning to 30°, maximum gain is 15.1 dBi on the E-plane, D-plane, and H-plane. Owing to its size, the anechoic chamber cannot reach the far-field distance at low frequency bands; therefore, the gain was measured from 400 MHz. In fact, the measured results of cross-polarization at 400 MHz are considerably higher than simulated results. We presume

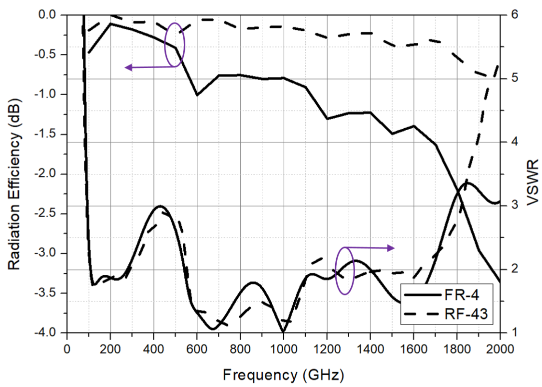

Fig. 11. Simulated radiation efficiency and VSWR of the proposed 4 × 4 finite array antenna with different materials of PCB.

TABLE I

COMPARISON WITH ULTRAWIDEBAND ARRAY ANTENNAS

Design	Bandwidth	Height (λ_{low})	θ_{max} (degree)	P_A
This Work	20.9:1*	0.067*	±30*	1.19*(2.15)
[12]	4.93:1*, 20.8:1	0.055	0	1.09
[7]	6.4:1	0.12	±60	2.24
[23]	5.5:1	0.088	E-plane: ±70 H-plane: ±55	2.84

* indicates the measured result of 4 × 4 finite array and all the others simulated result of unit cell.
The number in parentheses indicates the figure of merit when using the RF-43 board.

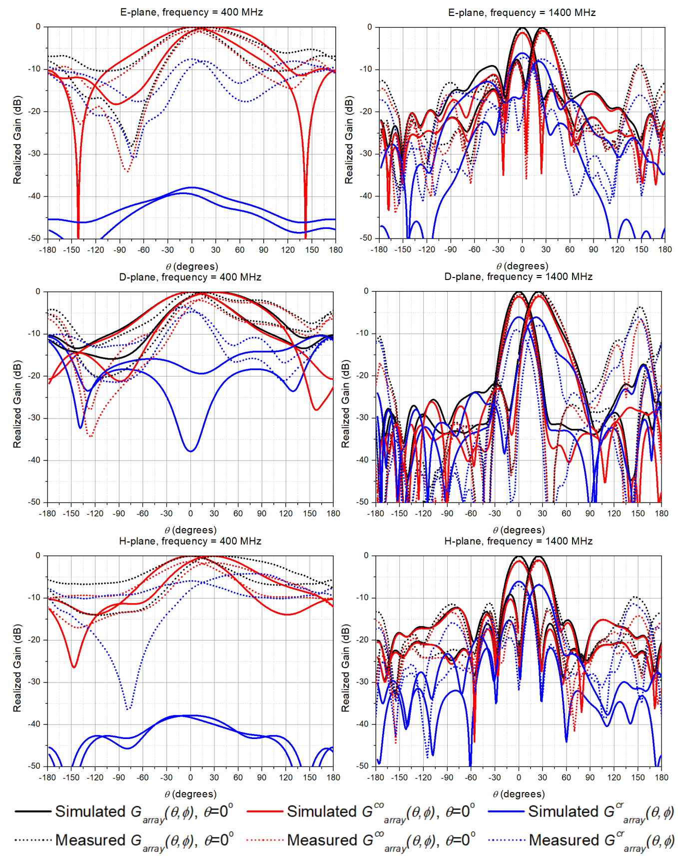

Fig. 12. Simulated and measured gain pattern of the proposed 4×4 finite array antenna at 400 and 1400 MHz on the E-plane ($\phi = 0°$), D-plane ($\phi = 45°$), and H-plane ($\phi = 90°$). The gain is normalized to $G_{array}(\theta, \phi)$.

that the reason for that is from the down-shift of operating band of the PC. In addition, the cross-polarization level is lower than the expected value when the array gains are compared in Fig. 2(b). The PEC side walls for the proposed 4 × 4 finite array decrease the cross-polarization level since the rotated y-polarization is weakened at the side elements due to the boundary condition. Thus, it is expected that increasing the number of elements in the finite array will increase the cross-polarization level.

Fig. 11 shows the radiation efficiency and VSWR of the proposed 4 × 4 finite array antenna designed with FR-4 and RF-43 substrates. Notice that the radiation efficiency is significantly different, particularly at high frequency bands since the loss tangent of FR-4 is approximately eight times larger than that of RF-43. The minimum radiation efficiency is higher than 92% at 1901 MHz when using the RF-43 board.

Fig. 12 shows the simulated and measured gain pattern for each types of polarization at 400 and 1400 MHz, respectively. The simulated results show that there is no polarization conversion at 400 MHz. Thus, $G^{co}_{array}(\theta, \phi)$ is almost the same with $G_{array}(\theta, \phi)$ to the main beam direction. Whereas, $G^{cr}_{array}(\theta, \phi)$ is comparable with $G^{co}_{array}(\theta, \phi)$ since the copolarization is converted to the cross-polarization at 1400 MHz. In fact, the back lobe level at 400 MHz is inevitably high because the electrical size of the GP (0.8 λ × 0.64 λ at 400 MHz) is small at low-frequency band.

The proposed array antenna is compared with the ultrawideband array antennas in Table I, in terms of their IBW, height, maximum scan angle θ_{max}, and figure of merit P_A. The figure of merit is calculated as follows [22]:

$$P_A = \frac{B|\log(1-\eta_{\min})|}{2\cos\theta_{\max}} \quad (8)$$

where $B = (f_{\max} - f_{\min})/\sqrt{f_{\max} f_{\min}}$, θ_{max} is the maximum scan angle, and η_{min} is the minimum total efficiency for the claimed IBW and scan range. The total efficiency includes impedance mismatch and ohmic losses. The proposed array antenna has lower ohmic loss without high ε_r superstrate compared to [12]. In contrast, the antennas in [7] and [23] show higher height and considerably narrower bandwidth.

IV. CONCLUSION

In this study, we proposed a TCDA with PC to overcome the bandwidth limitation at $h = 0.5\ \lambda$ and 1 λ of a conventional TCDA. The IBW of 91–1901 MHz (20.9:1) with frequency-dependent polarization was obtained. The height corresponds to 0.067 λ_{low} of the array antenna at the lowest operating frequency. Without superstrate, it can be used to scan the beam avoiding surface wave generation and it can be low-cost and low-weight. The measured maximum gain, $G_{array}(\theta, \phi)$ is 17.4 dBi within the operating band at broadside direction. When scanning to 30°, it is 17 dBi on the E-plane, D-plane, and H-plane. The proposed array antenna is expected to be successfully applied to wideband and beam-scanning applications.

REFERENCES

[1] J. Bang, J. Lee, and J. Choi, "Design of a wideband antipodal Vivaldi antenna with an asymmetric parasitic patch," *J. Electromagn. Eng. Sci.*, vol. 18, no. 1, pp. 29–34, Jan. 2018.

[2] S. Nelaturi and N. V. S. N. Sarma, “A compact microstrip patch antenna based on metamaterials for Wi-Fi and WiMAX applications,” *J. Electromagn. Eng. Sci.*, vol. 18, no. 3, pp. 182–187, Jul. 2018.

[3] H. A. Wheeler, “Simple relations derived from a phased-array antenna made of an infinite current sheet,” *IEEE Trans. Antenna Propag.*, vol. 13, no. 4, pp. 506–514, Jul. 1965.

[4] B. A. Munk, *Finite Antenna Arrays and FSS*. Hoboken, NJ, USA: Wiley, 2003.

[5] J. L. Volakis and K. Sertel, “Narrowband and wideband metamaterial antennas based on degenerate band edge and magnetic photonic crystals,” *Proc. IEEE*, vol. 99, no. 10, pp. 1732–1745, Oct. 2011.

[6] J. P. Doane, K. Sertel, and J. L. Volakis, “A wideband, wide scanning tightly coupled dipole array with integrated balun (TCDA-IB),” *IEEE Trans. Antennas Propag.*, vol. 61, no. 9, pp. 4538–4548, Sep. 2013.

[7] E. Yetisir, N. Ghalichechian, and J. L. Volakis, “Ultrawideband array with 70° scanning using FSS superstrate,” *IEEE Trans. Antennas Propag.*, vol. 64, no. 10, pp. 4256–4265, Oct. 2016.

[8] H. Lee and S. Nam, “A dual-polarized 1-D tightly coupled dipole array antenna,” *IEEE Trans. Antennas Propag.*, vol. 65, no. 9, pp. 4511–4518, Sep. 2017.

[9] S. Kim and S. Nam, “Bandwidth extension of dual-polarized 1-D TCDA antenna using VMS,” *IEEE Trans. Antennas Propag.*, vol. 67, no. 8, pp. 5305–5312, Aug. 2019.

[10] J. J. Lee, S. Livingston, and D. Nagata, “A low profile 10: 1 (200–2000 MHz) wide band long slot array,” in *Proc. IEEE Antennas Propag. Soc. Int. Symp.*, San Diego, CA, USA, Jul. 2008, pp. 1–4.

[11] Y. E. Erdemli, K. Sertel, R. A. Gilbert, D. E. Wright, and J. L. Volakis, “Frequency-selective surfaces to enhance performance of broad-band reconfigurable arrays,” *IEEE Trans. Antennas Propag.*, vol. 50, no. 12, pp. 1716–1724, Dec. 2002.

[12] W. F. Moulder, K. Sertel, and J. L. Volakis, “Superstrate-enhanced ultrawideband tightly coupled array with resistive FSS,” *IEEE Trans. Antennas Propag.*, vol. 60, no. 9, pp. 4166–4172, Sep. 2012.

[13] W. H. Syed and A. Neto, “Front-to-back ratio enhancement of planar printed antennas by means of artificial dielectric layers,” *IEEE Trans. Antennas Propag.*, vol. 61, no. 11, pp. 5408–5416, Nov. 2013.

[14] K. T. McDonald, “Reactance of small antennas,” Joseph Henry Lab., Princeton Univ., Princeton, NJ, USA, Tech. Rep., 2012.

[15] C. A. Balanis, *Antenna Theory: Analysis and Design*. Hoboken, NJ, USA: Wiley, 2016.

[16] B. Riviere, H. Jeuland, and S. Bolioli, “New equivalent circuit model for a broadband optimization of dipole arrays,” *IEEE Antennas Wireless Propag. Lett.*, vol. 13, pp. 1300–1304, Jun. 2014.

[17] X. Gao, X. Han, W.-P. Cao, H. O. Li, H. F. Ma, and T. J. Cui, “Ultrawideband and high-efficiency linear polarization converter based on double V-shaped metasurface,” *IEEE Trans. Antennas Propag.*, vol. 63, no. 8, pp. 3522–3530, Aug. 2015.

[18] S. Kim and S. Nam, “A compact and wideband linear array antenna with low mutual coupling,” *IEEE Trans. Antennas Propag.*, vol. 67, no. 8, pp. 5695–5699, Aug. 2019.

[19] M. N. Vouvakis and D. H. Schaubert, “Vivaldi antenna arrays,” in *Frontiers in Antennas: Next Generation Design & Engineering*. New York, NY, USA: McGraw-Hill, 2011, ch. 3.

[20] A. Ludwig, “The definition of cross polarization,” *IEEE Trans. Antennas Propag.*, vol. AP-21, no. 1, pp. 116–119, Jan. 1973.

[21] D. F. Kelley and W. L. Stutzman, “Array antenna pattern modeling methods that include mutual coupling effects,” *IEEE Trans. Antennas Propag.*, vol. 41, no. 12, pp. 1625–1632, Dec. 1993.

[22] J. P. Doane, “Wideband low-profile antenna arrays: Fundamental limits and practical implementations,” Ph.D. dissertation, Dept. Elect. Comput. Eng., Ohio State Univ., Columbus, OH, USA, 2013.

[23] A. O. Bah, P.-Y. Qin, R. W. Ziolkowski, Y. J. Guo, and T. S. Bird, “A wideband low-profile tightly coupled antenna array with a very high figure of merit,” *IEEE Trans. Antennas Propag.*, vol. 67, no. 4, pp. 2332–2343, Apr. 2019.